Spectroscopic Studies of Colloidal Solutions of Nanocrystalline $Ru(bpy)_3^{2+}$−Zeolite Y

Norma B. Castagnola and Prabir K. Dutta*

Department of Chemistry, The Ohio State University, 100 West 18th Avenue, Columbus, Ohio 43210

Received: October 6, 2000; In Final Form: December 5, 2000

Preparation of suspensions of $Ru(bpy)_3^{2+}$−zeolite Y has made it possible to use conventional optical transmission spectroscopic methods to examine the entrapped $Ru(bpy)_3^{2+}$ species within the zeolite. To prepare the suspensions, the surface hydroxyl groups of nanocrystalline zeolite Y were silylated using *n*-octadecyltrichlorosilane. The hydrocarbon sheath on the surface of the zeolites prevented agglomeration of the particles and made the surface hydrophobic enough for dispersion in toluene. The spectroscopic properties of the entrapped $Ru(bpy)_3^{2+}$ were measured via transmission techniques. For low levels of zeolite in the suspension (1 mg/10 mL), the scattering was low, and the absorption and fluorescence spectra of $Ru(bpy)_3^{2+}$-entrapped zeolite Y were quantitatively identical to the solution spectra with comparable $Ru(bpy)_3^{2+}$ concentrations. This suggests that all of the $Ru(bpy)_3^{2+}$ inside the zeolite is being sampled and the extinction coefficient of the complex is not altered upon incorporation inside the zeolite. The nature of the quenching mechanism in the $Ru(bpy)_3^{2+}$−viologen−zeolite Y system was studied by steady-state fluorescence and lifetime measurements, and it was determined to be mostly due to static quenching. Intrazeolitic electron transfer from the photogenerated viologen radical to $Ru(bpy)_3^{3+}$ was followed by flash photolysis, and information about the dynamics of the electron-transfer process was obtained. Comparison of the electron-transfer and quenching data with previous studies on zeolite samples examined by diffuse reflectance methods led to the conclusion that, in reflectance measurements, mostly the surface of the zeolite is sampled. The suspensions, on the other hand, provide a method to examine molecules inside the crystal. Overall, this study demonstrates that zeolite-entrapped complexes can be examined using transmission spectroscopic techniques by using nanocrystalline zeolites with modified surfaces.

Introduction

Spectroscopic studies on solid powdered materials such as zeolites commonly resort to diffuse reflectance techniques, which require special optical arrangements and precise methodology in sample handling and positioning, as well as appropriate theoretical treatments of the data to obtain quantitative results.[1] Several factors such as packing, particle size, light penetration depth, and angle of incident radiation are crucial to compare results between different samples. The extent of sampling through the solid sample is unknown. Several strategies have been reported in the literature to minimize the scattering and the development of transmission spectroscopic methods to examine zeolite samples. For example, by immersing the zeolite in a suitable nonabsorbing medium of similar refractive index, it was possible to largely remove the radiation loss due to scattering, and this has been demonstrated with sucrose solutions.[2] Recently, zeolites containing organic cations have been dispersed into organic polymers to form transparent films.[3,4] The films show transparency down to 220 nm, and intrazeolitic organic compounds could be studied using transmission techniques.[4] Although these transparent films are an important development, reactions than need access to the zeolite cannot be exploited because the crystals are embedded inside the matrix.

In this paper, we present a third strategy involving colloidal zeolite crystallites to make optically transparent solutions. Zeolite crystals in the nanometer range have been extensively investigated for their use in catalysis[5] and thin films[6] and as hosts for photochemical reactions.[7] So far, a variety of zeolites in the submicrometer size ranging from ∼8 to 200 nm have been synthesized.[8] In a previous study, we reported on the use of small crystals of zeolite X as photochemical hosts.[7] Even though an increase in the photochemical efficiency of charge separation across the zeolite−solution interface was observed, full advantage of the decrease in crystallite size was not realized because of considerable light scattering due to the extensive agglomeration of the zeolites. Here we report on the preparation of suspensions of $Ru(bpy)_3^{2+}$-entrapped nanocrystallite zeolite Y in toluene. To prevent agglomeration of the particles, the surface of the zeolite was modified by silylating the hydroxyl groups with a long hydrocarbon chain. All spectroscopic studies were done using transmission techniques under conditions typical of solution-based systems. The quenching mechanism in the $Ru(bpy)_3^{2+}$−viologen−zeolite Y system was confirmed to be static by steady-state fluorescence and lifetime measurements. Intrazeolitic electron transfer from viologen radical to $Ru(bpy)_3^{3+}$ was followed by flash photolysis. In addition to the spectroscopic advantages involving transmission measurements, sampling of all of the entrapped species inside the zeolite is possible, and because of the solution-based nature of the system, chemical studies with these crystals are also feasible.

Experimental Section

Synthesis of Zeolite Y. Colloidal crystals of zeolite Y with an average particle size of 100 nm were synthesized from clear homogeneous solutions following the synthesis procedure reported by Schoeman in 1994.[8a] A LUDOX SM silica sol (30.2 wt % SiO_2, 0.66 wt % Na_2O; Aldrich) was deionized (reduce Na^+) to a pH of 8.1 with a cationic ion-exchange resin, Dowex HCRS-E (Aldrich), in the H^+ form. A TMA−aluminate solution

10.1021/jp003677h CCC: $20.00
Published on Web 02/01/2001

was prepared from $Al_2(SO_4)_3 \cdot 18H_2O$ and TMAOH. A 19.7 g sample of $Al_2(SO_4)_3 \cdot 18H_2O$ (Baker) was dissolved in 75 mL of water, and the $Al(OH)_3$ was precipitated with a 26% NH_3 solution (Mallinckrodt). The gel was centrifuged, the supernatant was discarded, and the solid was redispersed in water to wash the excess ammonia and the sulfate ions. This procedure was repeated several times until the solid was free from sulfate ions. The sulfate-free $Al(OH)_3$ cake was dissolved in a solution containing 54 g of TMAOH, 25% aqueous solution, with stirring, yielding a clear mixture. This solution was added with mixing to 20 g of the partially deionized LUDOX sol to yield a clear solution with the molar composition

$(TMA)_2O$	Na_2O	Al_2O_3	SiO_2	H_2O
2.5	0.041	1.0	3.4	370

The synthesis mixture was heated without stirring in an oven at 100 °C. After a crystallization time of 7 days, the sample was washed and centrifuged for 2 h at a relative centrifugal force of 49000*g*. The product was washed three times and dried under vacuum for 5 h at room temperature. Yield: 0.7 g.

Characterization. The X-ray powder diffraction (XRD) pattern was recorded with a Rigaku Geigerflex diffractometer using Ni-filtered Cu Kα radiation (40 kV and 25 mA). The crystal size was calculated from the peak broadening using Scherrer's equation. Particle morphology was obtained using a JEOL 820 scanning electron microscope. The IR spectra (13 mm pellets, 0.25 mg of zeolite diluted in 100 mg of KBr) were acquired on a FTIR Mattson Cygnus 100 spectrophotometer. ^{29}Si and ^{27}Al solid-state NMR spectra were recorded on a Bruker AM 500.

Synthesis of $Ru(bpy)_3^{2+}$−Zeolite Y. The procedure has been previously reported for the synthesis of $Ru(bpy)_3^{2+}$−X(90).[7] The loading level of Ru complex was 1 per 15 supercages.

Silylation of the Zeolite Surface.[9] A 10 mM solution of octadecyltrichlorosilane in toluene was prepared under an inert atmosphere. The solvent was flushed with a stream of dry nitrogen for about 30 min before use. The silylating solution was used immediately. A 100 mg sample of $Ru(bpy)_3^{2+}$−Y was dispersed in 5 mL of toluene. The suspension was sonicated for 1 h to break the agglomerates and disperse the particles. A 20 mL portion of the silylating solution was added in the drybox, and the resulting solution was stirred at room temperature for 24 h. During this period the suspension was sonicated again for 30 min. The coated zeolite was removed by centrifugation and washed several times with toluene. The solid was dried under vacuum at room temperature and kept under nitrogen.

Sample Preparation. Samples for fluorescence, emission lifetime, and flash photolysis were ion-exchanged with N,N′-dimethyl-2,2′-bipyridinium (methyl viologen, MV^{2+}) prior to silylation. The loading levels of MV^{2+} were 3.33%, 10%, 20%, 85%, 110%, and 158%, with 100% denoting one molecule per supercage.

Instrumentation. Absorption spectra were recorded on a Shimadzu UV 265 spectrometer. Diffuse reflectance spectra were recorded using a Harrick diffuse reflectance attachment, with zeolite Y (100 nm) as the background. Fluorescence spectra were obtained on a Spex Fluorolog instrument, model F112AI. The sample was excited at 450 nm, and the data were acquired at right angles to the exciting beam. Lifetimes were measured using the second harmonic (532 nm) of a Quantel Nd:YAG Q-switched laser (1 Hz). The emission was monitored at a right angle to the excitation source using an Acton Research Corp. SpectraPro 275 single monochromator, a Hamamatsu R928 PMT, and a Tektronix DSA 601 digitizing signal analyzer, with a 11A52 two-channel amplifier. Transient absorption measurements were done with a modified setup of the time-resolved diffuse reflectance instrument (described in ref 15). The zeolite solution was sealed in a 1 cm quartz cell. The probe light directly passed through the sample, and the transmitted light was collected and focused into the Triplemate spectrometer. The excitation source was at 90° with respect to the probe light.

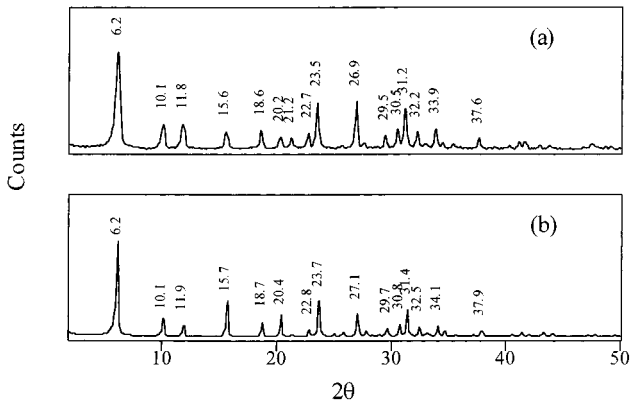

Figure 1. X-ray powder diffraction patterns of (a) as-synthesized nanocrystalline zeolite Y and (b) micrometer-sized zeolite Y.

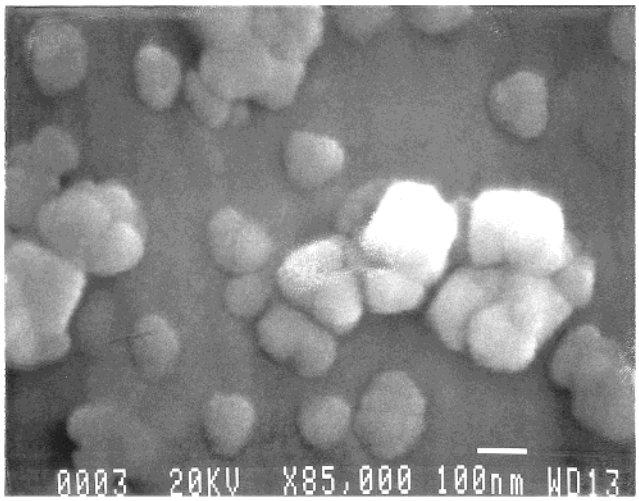

Figure 2. Scanning electron micrograph of as-synthesized nanocrystalline zeolite Y.

Results

Zeolite Synthesis and Characterization. ***Zeolite Y.*** The colloidal zeolite Y was synthesized from clear tetramethylammonium aluminosilicate solutions.[8a] Several attempts produced impurities of zeolite A, and to keep this contamination of zeolite A minimal, the Na^+ content had to be kept low.[8a] Figure 1a shows the XRD pattern of the zeolite. Peak broadening due to small particle size was observed when compared to micrometer-sized zeolite Y (Figure 1b), though it was not as pronounced as reported previously with nanocrystalline zeolite X.[7] On the basis of Scherrer's equation, an average crystallite size of 75 ± 15 nm was calculated from the peak at $2\theta = 6°$. Figure 2 shows a scanning electron micrograph of the nanocrystalline zeolite. The size of the discrete crystallites varied between 70 and 150 nm. Sonication of the sample improved dispersion of the particles. After calcination, extensive agglomeration was observed.

Further characterization of these crystallites was done by ^{29}Si and ^{27}Al NMR and infrared spectroscopy. The strongest peaks

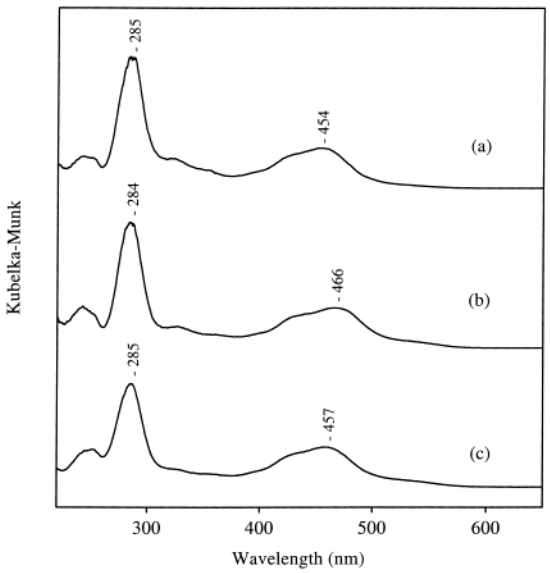

Figure 3. Diffuse reflectance spectra of (a) micrometer-sized $Ru(bpy)_3^{2+}$−zeolite Y, (b) nanocrystalline $Ru(bpy)_3^{2+}$−zeolite Y, and (c) silylated nanocrystalline $Ru(bpy)_3^{2+}$−zeolite Y.

in the ^{29}Si NMR spectrum were characteristic of $Si(OAl)_4$, $Si(OAl)_3$, and $Si(OAl)_2$ coordinations.[10] From the simulation of the experimental data based on Gaussian peak shapes, the intensities of the $Si(OAl)_n$ signals were retrieved and the Si/Al ratio was found to be 1.6, corresponding to zeolite Y. The ^{27}Al NMR showed a single symmetric peak around 60 ppm, characteristic of $Al(OSi)_4$ units. The infrared spectrum of the as-synthesized zeolite showed peaks from the entrapped tetramethylammonium ion (TMA) at 1490 (s), 1405 (m), 950 (sh), 777 (sh), and 711 (sh) cm^{-1}, in addition to the zeolite peaks. After calcination the TMA peaks were no longer present and the spectrum resembled that of zeolite Y. The strong Si−O vibrations around 950−1250 cm^{-1} are known to be sensitive to the Si/Al ratio of the framework.[11] The strongest peak for nanocrystalline zeolite X was reported at 987 cm^{-1} (Si/Al = 1.3),[7] for nanocrystalline zeolite Y we observe it at 1007 cm^{-1} (Si/Al = 1.6), and for zeolite Y we observe it at 1022 cm^{-1} (Si/Al = 2.4), which shows the expected shift to lower frequencies with increasing number of aluminum atoms. In conclusion, the NMR and infrared data confirm the formation of zeolite Y, while the XRD and scanning electron microscopy (SEM) data show that the crystallites are between 70 and 150 nm.

$Ru(bpy)_3^{2+}$−Nanocrystalline Y. The intrazeolitic Ru complex was synthesized following the modified procedure described in ref 7 using Ru $(NH_3)_6^{2+}$ as the starting reagent. The loading level of Ru was confirmed by elemental analysis to be 0.32% or 1 per 15 supercages. The $Ru(bpy)_3^{2+}$−nanocrystalline Y synthesis process did not lead to any decomposition of the zeolite, unlike the previous report with nanocrystalline X.[7] This thermal stability is a reflection of the Si/Al ratio of the framework, having increased from 1.3 for zeolite X to 1.6 for zeoliteY, rather than any intrinsic instability due to small crystallite size.

Figure 3 shows a comparison of the diffuse reflectance spectra of $Ru(bpy)_3^{2+}$−nanocrystalline zeolite Y (Figure 3b) and $Ru(bpy)_3^{2+}$−micrometer-sized zeolite Y (Figure 3a). To avoid effects due to differences in scattering, the samples were diluted (10% w/w) with micrometer-sized zeolite Y. The MLCT band of $Ru(bpy)_3^{2+}$ in the nanocrystals is red shifted 12 nm, although the electronic spectra of the Ru complexes extracted from both

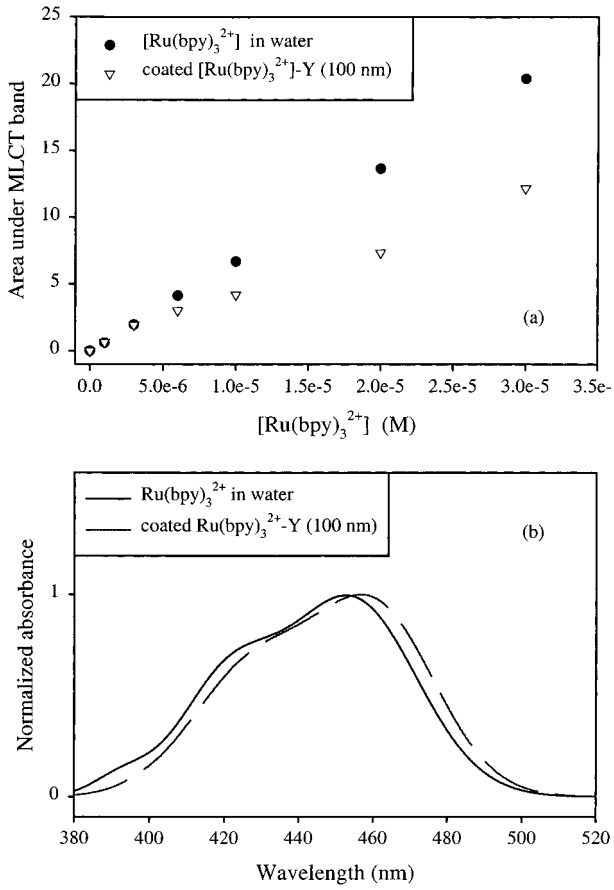

Figure 4. (a) Area under the 450 nm MLCT band versus the concentration of $Ru(bpy)_3^{2+}$ in solution (●) and in nanocrystalline zeolite Y suspensions (▽). (b) Comparison of the 450 nm MLCT band of $Ru(bpy)_3^{2+}$ in water and in nanocrystalline zeolite Y suspensions for $[Ru(bpy)_3^{2+}] = 3 \times 10^{-6}$ M.

the zeolite samples were superimposable and HPLC showed the presence of only one compound. Figure 3c shows the diffuse reflectance spectrum of the $Ru(bpy)_3^{2+}$−nanocrystalline zeolite Y sample whose surface hydroxyl groups have been silylated. The MLCT band has shifted back 9 nm, and now it is close to the λ_{max} of the micrometer-sized zeolites.

Spectroscopic Studies of Clear Colloidal Suspensions of $Ru(bpy)_3^{2+}$−Zeolite Y Nanocrystals. The following studies were done with toluene suspensions of surface-modified $Ru(bpy)_3^{2+}$−nanocrystalline zeolite Y using transmission techniques.

Absorption Measurements. The general features of the absorption spectra of aqueous $Ru(bpy)_3^{2+}$ and coated $Ru(bpy)_3^{2+}$−Y (100 nm) suspended in toluene are similar except for the fact that toluene strongly absorbs below 300 nm and masks the ligand-centered band that appears around 285 nm. A series of absorption and fluorescence measurements of both aqueous and zeolite suspensions with differing concentrations of $Ru(bpy)_3^{2+}$ were carried out. The concentration of $Ru(bpy)_3^{2+}$ in the zeolite suspension was adjusted by the amount of zeolite used rather than by altering the intrazeolitic $Ru(bpy)_3^{2+}$ concentrations. The concentration of $Ru(bpy)_3^{2+}$ in the suspension in terms of molarity was calculated from the known $Ru(bpy)_3^{2+}$ concentration in the zeolite and the amount of zeolite used to make the suspension as well as the volume of the solvent. A plot of the peak area versus $Ru(bpy)_3^{2+}$ concentration for the absorption band at 450 nm for both the solution and zeolite suspension is shown in Figure 4a. At concentrations of

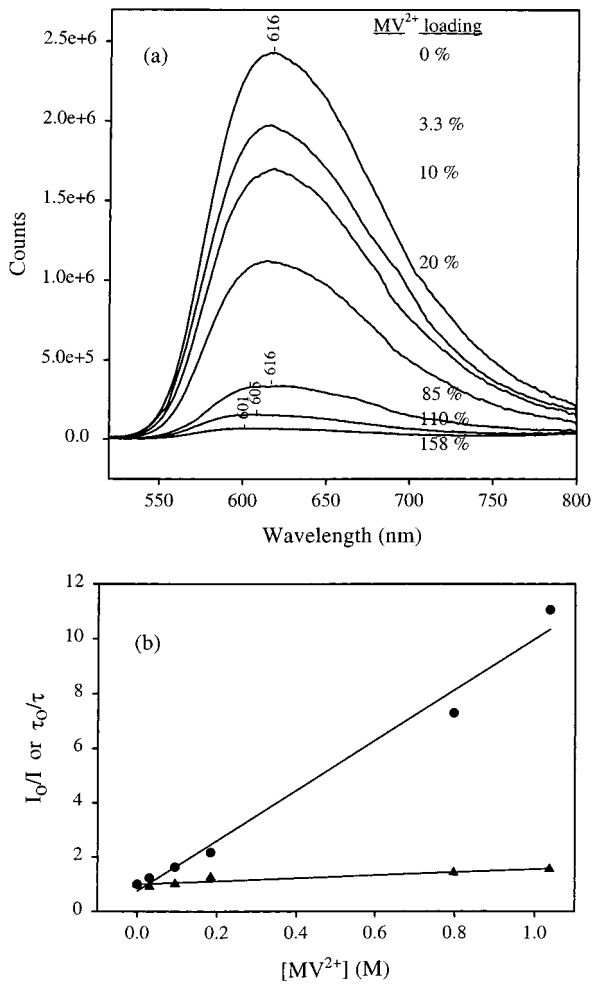

Figure 5. (a) Fluorescence quenching of $Ru(bpy)_3^{2+}$* at several MV^{2+} concentrations in nanocrystalline zeolite Y. The loading level of MV^{2+} is indicated (100% is 1 MV^{2+}/supercage). (b) I_o/I (●) and τ_o/τ (▲) versus [MV^{2+}] (M).

$Ru(bpy)_3^{2+}$ of 3×10^{-6} M and below (zeolite levels of 1 mg/mL), the areas under the peaks are identical for the homogeneous solution and zeolite suspension. Figure 4b shows the quantitative similarity of the charge-transfer band of $Ru(bpy)_3^{2+}$ for the aqueous and zeolite samples at the concentration of 3×10^{-6} M. Figure 4a also shows that, with increasing concentrations of the zeolite particles, there is deviation from the solution, and less and less of the $Ru(bpy)_3^{2+}$ in the zeolite is being sampled. This arises because of increased scattering, and is also evident from the fact that, for surface-modified micrometer-sized $Ru(bpy)_3^{2+}$−zeolite Y samples at concentrations of 3×10^{-6} M, the absorbance is only 43% of that observed in Figure 4b. For a suspension of uncoated $Ru(bpy)_3^{2+}$ nanocrystallites, the absorbance is only 70% of that of the coated sample. Even for the lowest amount of zeolite dispersions, the absorption spectra of the uncoated nanocrystallites or the coated micrometer-sized crystallites did not match the spectra with the corresponding $Ru(bpy)_3^{2+}$ solutions.

Similar results were obtained from fluorescence spectra. A quantitative match of the emission intensity at 610 nm was obtained with the coated nanocrystalline zeolite samples with zeolite loadings corresponding to $Ru(bpy)_3^{2+}$ concentrations of 3×10^{-6} M and solution samples.

Quenching Studies. The following studies were done with the $Ru(bpy)_3^{2+}$−nanocrystalline zeolite Y suspensions with the concentrations of zeolite around 5 mg/mL. The quenching of

TABLE 1: Fluorescence and Lifetime Quenching for Nanocrystalline $Ru(bpy)_3^{2+}$−MV^{2+}−Zeolite Y (Transmission Measurements)

[MV^{2+}], μmol/g	I_o/I	τ_o/τ	[MV^{2+}], μmol/g	I_o/I	τ_o/τ
0	1.0	1.0	96	2.3	1.2
16	1.2	0.9	415	7.3	1.4
49	1.6	1.0	540	11.0	1.7

TABLE 2: Fluorescence and Lifetime Quenching for Micrometer-Sized $Ru(bpy)_3^{2+}$−MV^{2+}−Zeolite Y (Reflectance Measurements)[14]

[MV^{2+}], μmol/g	I_o/I	τ_o/τ	[MV^{2+}], μmol/g	I_o/I	τ_o/τ
0	1.0	1.0	594	78.8	2.04
98	7.9	1.25	696	78.8	2.27

$Ru(bpy)_3^{2+}$* by MV^{2+} in nanocrystalline zeolite Y suspensions was determined by steady-state fluorescence and lifetime measurements. Fluorescence quenching of $Ru(bpy)_3^{2+}$* was recorded at different intrazeolitic MV^{2+} concentrations, and the spectra are shown in Figure 5. As expected, with increasing concentration of MV^{2+}, the emission intensity decreases. In addition, the λ_{max} of the emission band blue shifts at loadings higher than 1 MV^{2+}/supercage. The blue shift of the emission band at high viologen loadings is similar to what has been reported for micrometer-sized crystallites and attributed to the lack of solvent stabilization energy arising from the displacement of intrazeolitic water molecules upon ion exchange of the bipyridinium ions.[12]

Emission lifetimes of $Ru(bpy)_3^{2+}$−nanocrystalline zeolite suspensions were also measured, and the decay curves were fitted to Albery's dispersed kinetics model. Albery developed a model that assumes a Gaussian distribution of decay rates and has been shown to be appropriate for heterogeneous systems, including zeolites.[13] For the sample without any MV^{2+}, the values of γ and τ are 0.59 and 546 ns, respectively, and in agreement with previously reported results on the micrometer-sized zeolite Y crystallites.[14] Figure 5b is the plot of I_o/I and τ_o/τ versus intrazeolitic [MV^{2+}]. The quenching mechanism is mostly static in nature. Tables 1 and 2 summarize the MV^{2+} loading levels and the relative quenching values (I_o/I and τ_o/τ) for the zeolite suspensions as well as the comparison with previously published data by reflectance techniques on micrometer-sized zeolite Y.[14]

Laser Flash Photolysis. The intrazeolitic back electron transfer from $MV^{\bullet+}$ to $Ru(bpy)_3^{3+}$ was followed by transient spectroscopy using flash photolysis. The $Ru(bpy)_3^{2+}$ sample with the highest MV^{2+} loading (1.6 molecules/supercage) was used for these studies. The decay of the 395 nm band due to $MV^{\bullet+}$ was followed as a function of time. Figure 6a shows the transient absorption spectra at different time delays, and Figure 6b is the plot of the peak intensity at 395 nm as a function of time. The decay of the signal due to $MV^{\bullet+}$ was fit to the same model employed previously to explain the kinetics observed in micrometer-sized crystallites.[15] The following reactions were used for the modeling:

$$Ru(bpy)_3^{3+} + MV^{\bullet+}\ (\text{ext cage}) \xrightarrow{k_b} Ru(bpy)_3^{2+} + MV^{2+} \quad (1)$$

$$MV^{\bullet+} + MV^{2+} \xrightarrow{k_{hop}} MV^{2+} + MV^{\bullet+} \quad (2)$$

$$Ru(bpy)_3^{3+} + MV^{\bullet+} \xrightarrow{k_2} Ru(bpy)_3^{2+} + MV^{2+} \quad (3)$$

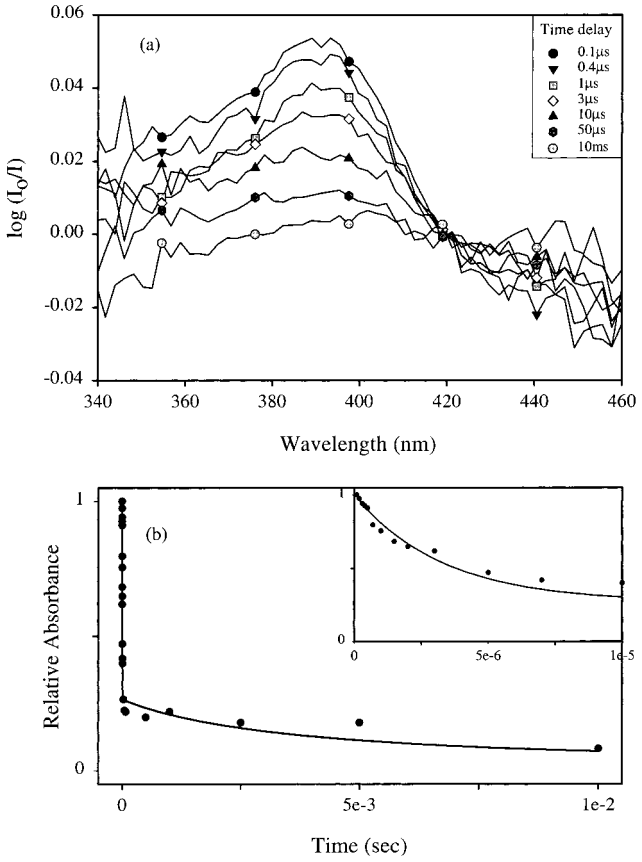

Figure 6. (a) Transient absorption spectra of nanocrystalline $Ru(bpy)_3^{2+}MV^{2+}$ (1.6 molecules/supercage)−Y (100 nm) suspended in toluene. (b) Decay of $MV^{\bullet+}$ as a function of time. The inset is the decay at early times. The solid line is the fit to the kinetic model explained in the text.

Reaction 1 involves the back electron transfer from the photogenerated $MV^{\bullet+}$ to $Ru(bpy)_3^{3+}$, reaction 2 is the self-exchange reaction between $MV^{\bullet+}$ and MV^{2+} that propagates the electron away from the $Ru(bpy)_3^{3+}$center, and reaction 3 is the eventual recombination of $Ru(bpy)_3^{3+}$ and $MV^{\bullet+}$ as the charge propagates through the zeolite. In Figure 6b, the solid line is the fit to the data (disappearance of $MV^{\bullet+}$) using the above model. From this fit, the k_b, k_{hop}, and k_2 rate constants were obtained to be 2.2×10^5 s^{-1}, 8.0×10^4 s^{-1}, and 1.0×10^3 $concn^{-1}$ s^{-1}, respectively. Table 3 is a comparison of the rate constants from colloidal solutions with those obtained by time-resolved diffuse reflectance on the micrometer-sized crystallites.[15]

Discussion

This discussion primarily contrasts the behavior of the intrazeolitic $Ru(bpy)_3^{2+}$ in the nanocrystallite samples versus those reported previously on micrometer-sized zeolite Y crystallites.

Nature of Nanocrystalline Y Suspensions. Comparison of the diffuse reflectance spectrum of $Ru(bpy)_3^{2+}$ in micrometer-sized and nanometer-sized zeolite Y aggregates at comparable loadings show that the visible charge-transfer band is red-shifted by about 12 nm in the smaller crystallites. The influence of $Ru(bpy)_3^{2+}$ concentration on the λ_{max} of the MLCT band has been reported in the literature.[16] Martin and co-workers observed a red shift in the MLCT band when $Ru(bpy)_3^{2+}$ was incorporated in layered zirconium phosphate sulfophenyl phosphonate at different concentrations. They attributed the red shift to interactions between $Ru(bpy)_3^{2+}$ molecules, since the λ_{max} of the MLCT band of $Ru(bpy)_3^{2+}$ shifts from around 452 nm in micromolar aqueous solutions to between 461 and 470 nm at concentrations of 4.4×10^{-4} M.[16a] Sykora et al. examined the diffuse reflectance spectra of $Ru(bpy)_3^{2+}$ inside the zeolite as a function of $Ru(bpy)_3^{2+}$ loading and discovered that increased loadings gave rise to a slight blue shift (5 nm) in the absorption spectra.[16b] In the nanocrystallites being examined here, the intrazeolitic $Ru(bpy)_3^{2+}$ loading is low (1 in 15 supercages), so the spectral shift is not arising from intrazeolitic effects between the $Ru(bpy)_3^{2+}$ molecules. We propose that the red shift arises in the agglomerated nanocrystallites due to $Ru(bpy)_3^{2+}$ on the surface of the crystallites interacting with each other. A simple calculation shows that the number of supercages in the first 10 nm of a 1 μm spherical zeolite particle is 3% of the total supercages, while for a 100 nm crystallite, the number jumps to 30%. In support of the argument that surface $Ru(bpy)_3^{2+}$ species are interacting, we find that, for the nanocrystallites with their surfaces modified by silylation, the λ_{max} is comparable to that of the micrometer-sized crystals, since the particles are less aggregated.

The quantitative similarity of the absorption spectra of the solution and nanocrystallite suspensions shown in Figure 4b at total $Ru(bpy)_3^{2+}$ concentrations of 3×10^{-6} M demonstrates several important results. First, the MLCT band remains unchanged. Second, its molar absorptivity in the zeolite remains unchanged, reflecting the aqueous intrazeolitic environment. Molar extinctions of $Ru(bpy)_3^{2+}$ adsorbed in porous Vycor glass as well as organic probes in zeolite−PDMS membranes have been reported to remain unaltered.[4,17] Third, all of the Ru complexes incorporated in the zeolite are being sampled by the light. However, with increased particle loading, scattering increases and there is deviation from the solution spectra. Silylation of the surface of the zeolite is necessary to keep the particles dispersed in toluene, for without the organic outer layer the particles tend to agglomerate very fast and the clusters rapidly settle. Settling is eventually observed with the organic-modified zeolites and forms an oily liquid at the bottom, which can be readily redispersed. In this study, we have chosen to work with a reasonably dilute loading of the $Ru(bpy)_3^{2+}$ in the zeolite (1 in 15 supercages) and have found that the upper limit for sampling the entire zeolite is a concentration of 1 mg/mL. However, even for this concentration of the zeolite, if a chromophore is present in every supercage, then as much as 4.5×10^{-5} M concentration of intrazeolitic chromophore can be studied.

Electron-Transfer Quenching by Viologens. We contrast here several aspects of the quenching studies on the nanocrystallite suspensions measured by transmission spectroscopic

TABLE 3: Comparison of the Rate Constants for the Decay of $MV^{\bullet+}$ in Nanocrystalline (Transmission Measurements) and Micrometer-Sized $Ru(bpy)_3^{2+}$−MV^{2+}−Zeolite Y (Diffuse Reflectance Measurements)[15]

sample	MV^{2+} loading (molecules/supercage)	k_b (s^{-1})	k_{hop} (s^{-1})	k_2 ($concn^{-1}$ s^{-1})
nanocrystalline Y	1.6	2.2×10^5	0.8×10^5	1.0×10^3
micrometer-sized Y	1.7	0.9×10^5	2.0×10^5	3.0×10^3

techniques with the reflectance studies on micrometer-sized crystallites reported in the literature.

First, we discuss the similarity between the two types of samples. The quenching mechanism of the excited $Ru(bpy)_3^{2+}$ by viologen in both cases is static,[14] which is not surprising considering that the diffusion of the viologens is slow since the zeolite architecture restricts the mobility of the quencher. The most significant difference in the two zeolite samples is the level of quenching of $Ru(bpy)_3^{2+}*$ by MV^{2+} (Tables 1 and 2 and Figure 5). For example, for a loading level of 1.1 MV^{2+}/supercage in the nanocrystallite, I_o/I is 11, while for 1.25 MV^{2+}/supercage in the micrometer-sized crystallite, it is on the order of 79.[14] From the absorption and fluorescence data with the colloidal solutions, it is evident that the interior of the zeolite is being sampled. Moreover, the surface derivatization by the hydrocarbon groups essentially ensures that viologen exchange on the outer surface of the zeolite is negligible. In the micrometer-sized crystallites, the surface is covered with viologen, serving as neutralizing cations for the aluminate on the framework. We interpret the higher quenching for the micrometer-sized crystallites as suggestive of the fact that the diffuse reflectance primarily samples the surface layers of the zeolite, which is enriched in viologen.

The surface sampling of the diffuse reflectance measurements also serves to explain the magnitude of the k_b and k_{hop} rate constants related to the back electron transfer from the $MV^{\bullet+}$ to $Ru(bpy)_3^{3+}$ (Table 3). The packing of the viologens is crucial in determining the viologen self-exchange rate constant (k_{hop}).[15] The enhanced concentration of the viologens on the surface of the micrometer-sized crystallites leads to a higher k_{hop} value, which is reflected in the diffuse reflectance measurements. For the nanocrystallites, the interior of the crystal is sampled and the value of the k_{hop} is lower. The back-electron-transfer rate constant from $MV^{\bullet+}$ to $Ru(bpy)_3^{3+}$ (k_b) is also consistent with the surface enrichment of the viologen. The k_b for micrometer-sized crystallites is smaller than that for the nanocrystalline material because the viologens on the surface are less constrained than the viologens packed in the supercages, and is consistent with the k_b values noted in an earlier study as a function of viologen loading.[15]

Conclusion

The surface of ~100 nm zeolite Y particles was modified by silylation of the hydroxyl groups with octadecyltrichlorosilane. Dispersion of these hydrophobic particles in toluene yielded transparent solutions, which were successfully studied by transmission spectroscopic techniques. At and below a certain level of dispersion of the zeolites (1 mg/mL), scattering is sufficiently low, such that all of the entrapped $Ru(bpy)_3^{2+}$ in the zeolite is sampled by optical spectroscopy. Intrazeolitic electron transfer was examined for the $Ru(bpy)_3^{2+}-MV^{2+}-$zeolite Y nanocrystallite dispersions. Marked differences were found for the zeolite suspensions sampled by transmission techniques and previous studies based on diffuse reflectance measurements on micrometer-sized crystallites, leading us to the conclusion that the diffuse reflectance measurements sample primarily the surface of the crystallites. Since the MV^{2+}-exchanged zeolites have an enriched MV^{2+} surface layer in the case of micrometer-sized crystallites, the quenching efficiency of $Ru(bpy)_3^{2+}*$ by MV^{2+} and the viologen self-exchange rate constants were higher in micrometer-sized crystallites as compared to the nanocrystalline dispersions. For both zeolite samples, the quenching mechanism for $Ru(bpy)_3^{2+}-MV^{2+}-$zeolite Y was found to be static, since the mobility of the MV^{2+} is highly restricted. The results obtained via transmission measurements from the colloidal solutions are more representative of the total sample, since all of the intrazeolitic species are being measured.

Acknowledgment. We acknowledge the Department of Energy, Basic Sciences Division, for funding this research.

References and Notes

(1) Kortüm, G. Reflectance Spectroscopy; Springer-Verlag: New York, 1969.

(2) Persaud, L.; Bard, A. J.; Campion, A.; Fox, M. A.; Mallouk, T. E.; Webber, S. E.; White, J. M. *J. Am. Chem. Soc.* **1987**, *109*, 7309.

(3) Vankelecom, I. F. J.; Dotremont, C.; Morobe, M.; Uytterhoeven, J. B.; Vandecasteele, C. *J. Phys. Chem. B* **1997**, *101*, 2154.

(4) Alvaro, M.; Garcia, H.; Corrent, S.; Scaiano, J. C. *J. Phys. Chem. B* **1998**, *102*, 7530.

(5) Yamamura, M.; Chaki, K.; Wakatsuki, T.; Okado, H.; Fujimoto, K. *Zeolites* **1994**, *14*, 643.

(6) (a) Jung, K. T.; Shul, Y. G. *Chem. Mater.* **1997**, *9*, 420. (b) Lovallo, M. C.; Tsapatsis, M.; Okubo, T. *Chem. Mater.* **1996**, *8*, 1579.

(7) Castagnola, N. B.; Dutta, P. K. *J. Phys. Chem. B* **1998**, *102*, 1696.

(8) (a) Schoeman, B. J.; Sterte, J.; Otterstedt, J.-E. *Zeolites* **1994**, *14*, 110. (b) Otterstedt, J.-E.; Sterte, J.; Schoeman, B. J. International Patent, WO 94/05597, 1994. (c) Engel, S.; Kynast, U.; Unger, K. K.; Schuth, F. *Stud. Surf. Sci. Catal.* **1994**, *84*, 477. (d) Madsen, C.; Jacobsen C. J. H. *Chem. Commun.* **1999**, 673. (e) Zhu, G.; Qiu, S.; Yu, J.; Yasuhiro, S.; Fengshou, X.; Xu, R.; Terasaki, O. *Chem. Mater.* **1998**, *10*, 1483.

(9) Singh, R.; Dutta, P. K. *Microporous Mesoporous Mater.* **1999**, *32*, 29.

(10) Klinowski, J.; Ramdas, S.; Thomas, J. M.; Fyfe, C. A.; Hartman, J. S. *J. Chem. Soc., Faraday Trans. 2* **1982**, *78*, 1025.

(11) Breck, D. W. Zeolite Molecular Sieves; Wiley and Sons: New York, 1974.

(12) Coutant, M.; Le, T.; Castagnola, N.; Dutta, P. K. *J. Phys. Chem. B* **2000**, *104*, 10783.

(13) (a) Albery, W. J.; Bartlett, P. N.; Wilde, C. P.; Darwent, J. D. *J. Am. Chem. Soc.* **1985**, *107*, 1854. (b) Li, Z.; Mallouk, T. E. *J. Phys. Chem.* **1987**, *91*, 643.

(14) Dutta, P. K.; Turbeville, W. *J. Phys. Chem.* **1992**, *96*, 9410.

(15) Vitalle, M.; Castagnola, N. B.; Ortins, N. J.; Brooke, J. A.; Vaidyalingam, A.; Dutta, P. K. *J. Phys. Chem. B* **1999**, *103*, 2408.

(16) (a) Colon, J. L.; Yang, C.-Y.; Clearfield, A.; Martin, C. R. *J. Phys. Chem.* **1988**, *92*, 5777. (b) Sykora, M.; Kincaid, J. R.; Dutta, P. K.; Castagnola, N. B. *J. Phys. Chem. B* **1999**, *103*, 309.

(17) Shi, W.; Wolfgang, S.; Strekas, T. C.; Gafney, H. D. *J. Phys. Chem.* **1985**, *89*, 974.